Electroreduction of CO$_2$ to Formate with low overpotential using Cobalt Pyridine Thiolate Complexes

Subal Dey,[a],[b] Tanya K Todorova,[b] Marc Fontecave,[b]* and Victor Mougel[a],[b]*

[a] Department of Chemistry and Applied Biosciences, ETH Zürich, Vladimir-Prelog-Weg 1-5, 8093 Zürich (Switzerland)
[b] Laboratoire de Chimie des Processus Biologiques, UMR 8229 CNRS, Collège de France, Paris, Sorbonne Université, PSL Research University, 11 Place Marcelin Berthelot, 75231 Paris, Cedex 05 (France)
E-mail: marc.fontecave@college-de-france.fr (M. Fontecave)
E-mail: mougel@inorg.chem.ethz (V. Mougel)

Abstract: Electrocatalytic CO$_2$ reduction to value-added products provides a viable alternative to the use of carbon sources derived from fossil fuels. Nevertheless, the ability to carry out these transformations at reasonable energetic costs, e.g. with low overpotential, remains a significant challenge. Molecular catalysts offer a great option in this context, as fine control of their activity and selectivity can be obtained via the tuning of their coordination sphere and ligand set. To this end, we investigated here a series of cheap cobalt(III) pyridine-thiolate complexes as electrocatalysts for CO$_2$ reduction. The effect of the ligands and proton sources on activity was examined. We were able to identify [bipyridine-*bis*-(2-pyridinethiolato)-cobalt(III)-hexaflurophosphate] as a highly selective catalyst for formate production operating at a very low overpotential of 110 mV to achieve a TOF of 10 s^{-1}. Detailed electrokinetic analysis coupled with density functional theory allowed establishing a mechanistic pathway for these catalysts, highlighting the role of key metal hydride intermediates. The catalysts deactivate via the formation of stable Co carbonyl complexes, but we demonstrated that the active species could be regenerated upon oxidation and release of coordinated CO ligands.

Introduction

Carbon dioxide can be used as a carbon source alternative to fossil-fuels for the production of energy-dense chemicals by electrolysis utilizing renewable energy sources. The inherent stability of CO$_2$ has triggered a large number of studies aimed at developing active catalysts to promote its reduction.[1] Early studies have focused on low-valent rare metal catalysts (e.g. Re,[2] Ru,[3] Ir,[4] Rh,[5]) and have been more recently extended to earth-abundant transition metals (e. g. Mn,[6] Fe,[7] Co,[8] Ni[9]). This large number of molecular catalysts has enabled understanding the mechanistic pathways for CO$_2$ reduction and elucidating the electronic factors responsible for the catalyst selectivity to either CO or HCOOH.[1] However, the vast majority of them still suffer from high overpotentials (generally 300-800 mV).[1, 10]

The major advantage of molecular catalysts is that they offer an easy modulation of their catalytic properties by tuning the electronics of the ligands. Yet surprisingly, in the context of CO$_2$ reduction a vast majority of the reported catalysts show very little variation in their 1st coordination sphere, where nitrogen-based donor ligands are used in most cases. Despite being ubiquitous in the enzymatic systems competent for CO$_2$ transformation (carbon monoxide dehydrogenase[11] and formate dehydrogenase[12]), thiolate ligands had not been used for the design of CO$_2$ reduction catalysts until recently.[13] Thiolate ligands are soft Lewis bases with σ and π−donation properties, providing increased electron density on reduced metals while maintaining strong metal-ligand covalency. These two factors are beneficial to the reactivity of the reduced complexes with CO$_2$. However, because of their anionic character, thiolate ligands also disfavor the reduction of the complex, as the active species require more cathodic potential to be generated. This can, in turn, result in substantial overpotentials as well as less effective catalysts in terms of turnover numbers (TONs). Here, we show that highly active Co-based CO$_2$ reduction molecular catalysts can be obtained via the modulation of the electronic influence of anionic thiolate ligands with neutral nitrogen ligands. We prepared a series of 2-pyridinethiolate Co complexes notably combined with substituted bipyridine (bpy) ligands. These complexes, obtained in one synthetic step from cheap commercially available reagents, are capable of catalyzing electrochemical CO$_2$ reduction at very low overpotential with high selectivity towards carbon-based products. We report the investigation of their catalytic activity in the presence of different proton sources and ligand sets and propose a mechanistic explanation to the observed activity supported by theoretical calculations.

Results and Discussion

Synthesis and Characterization

We investigated here the series of Co complexes presented in Scheme 1. [bipyridine-*bis*-(2-pyridinethiolato)-cobalt(III)-hexaflurophosphate] (**1**) and [4,4´-bismethoxy-bipyridine-*bis*-2-pyridinethiolato-cobalt(III)-hexaflurophosphate] (**2**) were synthetized in 67 and 83% yield respectively by addition of 2 equivalents of sodium pyridine-2-thiolate to a methanol solution of [bipyridyl-dichloro-cobalt(II)], by analogy with reported procedures for the corresponding nickel(II) complexes[14] and subsequent aerobic oxidation. The perchlorate analogue of **1** had been previously prepared using a different synthetic route but had not been extensively characterized.[15] Complex **3** [*tris*-2-pyridinethiolato-cobalt(III)] was synthesized in 61% yield *via* the salt metathesis reaction of 3 equivalents of sodium pyridine-2-thiolate and Co(II)Cl$_2$ in methanol followed by aerobic oxidation.

1, R = H
2, R = OMe   **3**
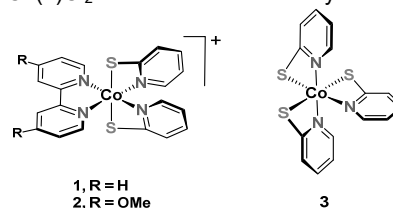
Scheme 1: Co pyridine-thiolate complexes **1-3**.

Complexes **1-3** were fully characterized by elemental analysis, UV-Vis, ^{1}H-NMR, HR-MS and single crystal X-ray crystallography. The X-ray single crystal structures of the complexes **1-3** are shown in Figure 1. Both complexes **1** and **2** crystallize in a distorted octahedral geometry with the S ligands *trans* to each other in the axial positions (S-Co-S angle = 165°) and the four N positioned in the equatorial plane. The Co-S bond distances of 2.304(4) Å and 2.288(1) Å and the average Co-N bond distances of 1.932(2) Å and 1.929(2) Å for **1** and **2** are in good agreement with previously reported low-spin Co(III) complexes bearing thiolate[16] and pyridine[17] ligands. The main difference between the structures of **1** and **2** resides in the C-C bond distance between the two pyridine rings of the bpy moiety of 1.467 and 1.486 Å for **1** and **2** respectively, correlating with the stronger electron donating properties of the -OMe groups. Due to the asymmetry induced by its ligand set, complex **3** deviates slightly more from octahedral geometry, having two S ligands in axial positions (S-Co-S angle = 164°) and an equatorial plane defined by the third sulfur and the three nitrogen ligands. The notable difference of this new series of complexes with previously reported Fe(II)[18] and Ni(II) analogues[19] is the much shorter M-S bond distances consistent with the +III oxidation state of Co.
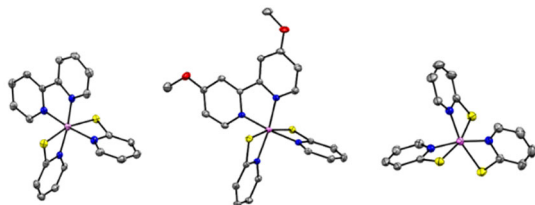

Figure 1: Solid-state molecular structure of complexes **1-3** (*left to right*) Counter anion, interstitial solvent molecules and H atoms were omitted for clarity. Carbon (grey), cobalt (pink), nitrogen (blue) and sulfur (yellow) atoms are represented with 50% probability ellipsoids.

^{1}H NMR spectra confirm the diamagnetism of these complexes, as expected for low spin Co(III) complexes. UV-Vis data (Figure S1) showed three main absorptions peaks for **1** at 313, 377 and 613 nm respectively. Very similar absorption features are found for in the UV-Vis spectrum of complex **2** (326, 373 and 607 nm), while that of complex **3** shows a strong absorption at 280 mm along with three consecutive shoulders at 298, 324, 365 and a broad band at 700 nm. The broad low energy maxima with lower intensity ($\varepsilon < 100$ L mol-1 cm-1) at ~610 nm for **1** and **2** and at 700 nm for **3** are attributed to spin-allowed *d-d* transitions, as expected for pseudo-octahedral low-spin Co(III) complexes.[20] The red shift of the thiolate-to-metal charge transfer in **3** suggests an increased electron density at the metal center, in agreement with the presence of the three anionic thiolate ligands.

Additional high energy absorptions with high ε observed for all complexes can be attributed to the charge transfers from thiolate to metal and the inter ligand charge transfer ($\pi - \pi^*$).

Electrochemical Data:

a. Cyclic voltammetry under Argon: The electrochemical properties of the complexes were investigated by cyclic voltammetry (CV) in 0.1 M (^{n}Bu)$_4$NPF$_6$ anhydrous acetonitrile solution under an Argon atmosphere (Figure 2a, and Table 1). All complexes **1-3** presented a first reversible reduction wave at a half-wave potential ($E_{1/2}$) (determined as the average of the cathodic peak *potential E_p* and the anodic peak potential E_a) between -0.77 V and -1.1 V (all potentials are reported here *vs.* Fc/Fc+) and peak to peak separation values (ΔE_p) between 75 and

97 mV. By analogy with previously reported data for complex **1**, we assigned this redox wave to a Co[III/II] process.[21]
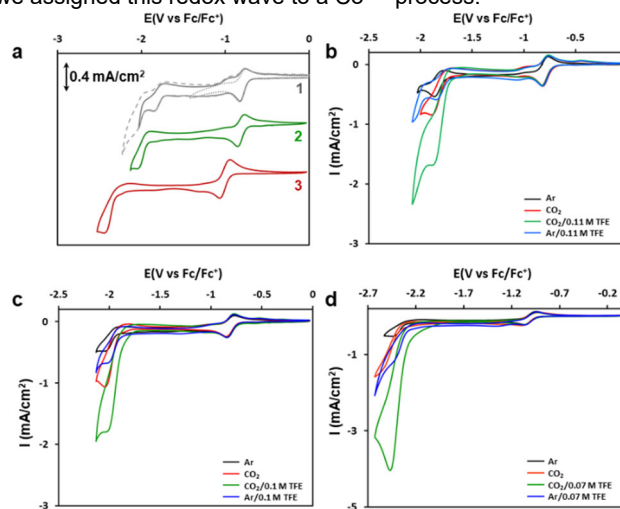

Figure 2: Electrochemical behaviour of the complexes. a. Cyclic voltammograms of complex **1**, **2** and **3** under argon. CV scans for various potential windows are overlaid (dashed lines) for complex **1** only. b, c, d are the overlay of the CV responses for **1, 2** and **3** respectively under catalytic condition, under argon in the absence (black) or presence (blue) of TFE, in the presence of CO_2 (red) and in the presence of TFE and CO_2 (green). All data were collected using 1 mM solution of the complexes in CH_3CN/0.1 M (^{n}Bu)$_4$NPF$_6$ at 100 mVs-1 scan rates using GC working electrodes.

Table 1. Electrochemical characteristics of complex **1-3**.

Complex	$E_{1/2}$ [III/II] (V)	$E_{1/2}$ [II/I] (V)[a]	ΔE_p [III/II][b] (mV)	D_{cat}[III/II],[b] cm^{2}s-1
1	-0.77	-1.85	75	3.3 10-6
2	-0.81	-2.02	82	3.1 10-6
3	-1.02	-2.35	97	3.0 10-6

[a] The peak to peak separation (ΔE_p) for Co[II/I] processes are not provided due to large irreversibility of the CVs. [b] The diffusion coefficients are mentioned for the Co[III/II] processes, in cathodic scan.

On further cathodic scan, two successive irreversible one-electron redox processes appear for **1** at -1.85 V and -2.05 V respectively (Figure 2a, dashed line). The redox process at -1.85 V is assigned as reduction of Co(II) to Co(I) species, while the process at -2.05 V is attributed to the reduction of the bpy ligand, in agreement with previously reported values for Ni or Fe complexes containing bpy ligands.[22] We ascribed the increased irreversibility of the Co[II/I] process at lower scan rates (Figure S2) to the dissociation of a pyridine-thiolate ligand, as observed for corresponding Ni analogues where dissociation of the pyridine moiety of 2-pyridinethiolate ligand had been established (Scheme 2).[14] This hypothesis is further supported by the appearance of a new pre-wave to the Co(II) to Co(III) oxidation feature at -0.95 V on anodic scan and assigned to the oxidation of this five coordinated Co(I) species. Complex **2** presents a similar redox behavior with an overall cathodic shift of the $E_{1/2}$ values (Figure 2a green, Figure S3 and Table 2), in agreement with the electron-donating properties of the –OMe groups. This has a stronger impact on the most reduced state, a cathodic shift of 170 mV being observed for $E_{1/2}$ (Co[I/I]). The tris pyridine-thiolate complex **3** shows a reversible redox peak at a more cathodic value of -1.04 V attributed to the Co[III/II] couple (Figure 2a red and Figure S3). An

irreversible feature was observed at the very cathodic potential of -2.35 V. We hypothesize that this irreversible feature is associated with a permanent ligand dissociation from the Co(I) center. This hypothesis is further confirmed by the appearance of an additional oxidation wave at ca. -0.4V at the higher scan rates for **1** and **2** (Figure 2 and Figures S2-S3), assigned to the oxidation process of the thus generated pentacoordinated Co(II) complexes. The observation of ligand dissociation events for all complexes suggests that open coordination sites are generated upon reduction, a prerequisite for binding an exogenous ligand (e. g. CO_2, proton etc.). All the complexes show free diffusion behavior in solution according to Randles-Sevcik plot, which allows homogeneous electrocatalytic investigations to be performed (*see ESI for details*).
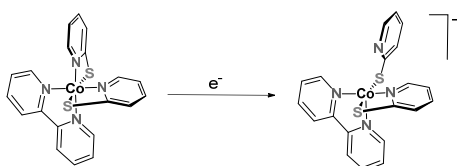
Scheme 2: Proposed redox assisted pyridine dissociation for the complexes.

DFT optimization of complex **1** showed that it has a singlet ground state and its computed geometry is in excellent agreement with the experimental X-ray single crystal structure (bond distances are within 0.01 Å and bond angles are within 1° of the corresponding values in the crystal structure) (Table S2). Its one-electron reduction leads to the formation of a Co^{II} species, **1$_{red1}$**, which has a quartet spin state that is 2.4 kcal mol^{-1} lower in energy than the doublet state. Our DFT calculations show that addition of an extra electron in **1** results in ~0.2 Å elongation of all six Co–L distances in the high-spin structure **1$_{red1}$**, while in the low-spin **1$_{red1}$** the Co–S bonds are elongated to as much as 0.39 Å, and only ~0.01 Å for the Co–N bonds. The electron resides on the Co center (Figure S5B), which has a Mulliken spin density of 2.63, implying an oxidation state of +2. One-electron reduction of **1$_{red1}$** generates a high-spin triplet Co^I species **1$_{red2}$** (open-shell singlet is 14 kcal mol^{-1} higher in energy) as illustrated by the orbital analysis (Figure S5C). Computations indicate the existence of two different geometries, i.e., **1$_{red2}$** and **1$_{red2'}$** that are less than 1 kcal mol^{-1} different in energy. **1$_{red2}$** preserves the coordination sphere around the Co^I center, but the two Co–S bond lengths are further elongated by 0.24 Å, while the Co–N distances are shortened by 0.17 Å (Table S2). In contrast, in **1$_{red2'}$** one Co–N$_{PyS}$ bond is cleaved, while the other Co–N bond distances are almost unchanged, and Co–S ones are shortened by ~0.2 Å, in agreement with the ligand dissociation process mentioned above.

b. Catalytic behavior under CO$_2$: The electrochemical CO_2 reduction ability of these complexes was investigated in CO_2 saturated (~0.23 M) CH_3CN solution. The electrochemical data for

all complexes are given in Figure 2. In the presence of CO_2, irreversible features with current enhancement were observed for complexes **1-3** at the potential of the $Co^{II/I}$ redox couple (red traces of Figure 2b, 2c and 2d and half-peak potentials given in Table 2). Half-peak potential values suggest that CO_2 activation occurs on Co(I) complexes. The modest current enhancement encouraged us to explore the use of proton sources to enhance the rates and lower the overpotential of the reaction.[6a, 23] Using complex **1** as a prototypical catalyst to identify the best reaction conditions, we observed that the I_{cat}/I_p value was substantially increased upon addition in the electrochemical solution of 2,2,2-trifluoroethanol (TFE), H_2O, or phenol (PhOH). The largest value was observed using TFE (see Figures S6-S8 and ESI for details). The catalytic performances of **1** were hence investigated by 2 h controlled potential electrolysis (CPE) at -1.83 V in the presence of these proton sources (Figure S9-S10 and Table S3). The highest overall FY for CO_2 reduction value of 64 % (7 % of CO and 57 % of HCOOH, together with 19 % for H_2) was obtained using TFE, which was thus chosen for the investigation of the catalytic activity of the other complexes described here. With respect to complex **1**, 2 h CPE at -1.98V of a CO_2-saturated solution of complex **2** in the presence of TFE (Figure S13a) revealed an increase of the selectivity for CO_2 reduction (70 % FY) accompanied by a lower undesired H_2 evolution (10 % FY), yet at the cost of a more cathodic potential ($E_{cat/2}$ = -1.93 V). Product analysis after 2 h CPE for **3** at -2.33 V (Figure S13b) revealed high selectivity for HCOOH (57 % FY) with low CO and H_2 generation (2.5 % and <1% respectively, Table 2).

The high selectivity of complex **3** is nevertheless counterbalanced by its low total FY of ca. 60 % and very cathodic catalytic potential ($E_{cat/2}$ = -2.35 V). This low total FY goes along with lower turnover numbers (TONs) and a fast decrease of the current during CPE (Figure S13b and table S3), highlighting the lower stability of complex **3** with respect to complexes **1** and **2** (Table 2).

For all three catalysts and all proton sources, the total FYs reported above are below unity and vary between 61 and 83 %. These low total FYs result from the deactivation of the catalysts in catalytic conditions, further discussed in the section below "catalyst deactivation mechanism".

c. Benchmarking of the Catalysts: In order to compare their catalytic performances, we evaluated the CO_2 reduction kinetics of complexes **1-3** by determining their maximum turnover frequency (TOF$_{max}$, see ESI for details). TOF$_{max}$ values of 27.5 s^{-1} and 29.5 s^{-1} were obtained for **1** and **2** respectively, indicating that the introduction of electron-donating substituent on the bpy moiety does not significantly increase the rate of the reaction despite driving the operating potential to more cathodic values. By contrast, the presence of a third pyridine-thiolate ligand strongly influenced the reaction kinetics, with a TOF$_{max}$ value of 178 s^{-1} determined for complex **3**. We benchmarked the catalytic performances of catalysts **1-3** against other molecular catalysts

Table 2. Comparative catalytic parameters for complex **1-3** in presence of CO_2 and TFE.

Catalyst	$E_{cat/2}$[a]	TFE conc.[b]	TOF$_{max}$ (s^{-1})[c]	Total TON[d]	FY$_{CO}$ (%)[d]	FY$_{formate}$ (%)[d]	FY$_{H2}$ (%)[d]	η_{10s-1} [e]
1	-1.74	0.11 M	27.5	5.4	7	57	19	110
2	-1.93	0.07 M	29.5	5.1	6	64	10	280
3	-2.35	0.07 M	178	2.4	2.5	57	< 1	600

using a catalytic Tafel plot, presented in Figure 3 (see ESI for details on the construction of the Tafel plot).[24] The catalytic Tafel plot allows examining the catalytic performances against both kinetic (TOF_{max}) and thermodynamic (overpotential, η) descriptors. It should be noted here that the TOF_{max} and Tafel plot could be confounding as the complexes reported in this manuscript show selectivity for HCOOH below unity. Nevertheless, plotting the turnover frequencies for formate determined from the CPE at different applied overpotentials on the Tafel plot highlights their overall match with the logTOF-η plots determined by CV measurements (Figure 3, see ESI for details). The TOF values determined from the CPE data are slightly higher than those determined by CV measurements, in agreement with the additional convection resulting from the stirring applied during CPE experiments. This confirms the validity of the Tafel plot for complexes **1-3** and enables comparison with previously reported catalysts for the reduction of CO_2 to HCOOH, namely Ir(POCOP),[4] $HFe_4N(CO)_{12}$,[25] $Ni(qpdt)_2{}^{2-}$,[13a] $FeN_5Cl_2{}^+$,[26] $Pt(dmpe)_2{}^{2+}$,[27] $IminobpyCo^{3+}$[28] and $CpCo(P_2N_2)^{2+}$.[8c]
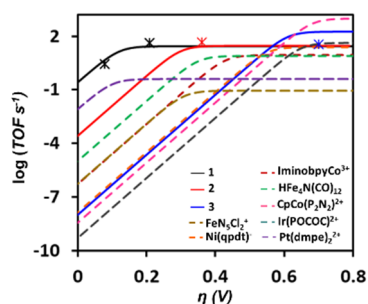

Figure 3: Catalytic Tafel plot for complex **1** (black line), **2** (red line) and **3** (blue line). The data are presented in comparison with other selective molecular catalysts for the reduction of CO_2 to HCOOH (dashed lines, see inset). Crosses represent the TOFs for formate determined from CPE data. Values and conditions are given in ESI.

It clearly appears that complex **1** stands among the best reported CO_2 to HCOOH catalysts: achieving a TOF of 10 s^{-1} requires less than 110 mV overpotential for **1**, which is the lowest value reported so far. While the catalysts Ir(POCOP), $CpCo(P_2N_2)^+$ and $Ni(qpdt)_2{}^{2-}$ show relatively higher TOF_{max} values, in the same range than that for **3**, this comes at the cost of a substantial overpotential (~600 mV, Table 2).[4, 8c, 13a]

d. Catalyst deactivation mechanism: As described above, the complexes reported here all present total FYs significantly below unity. This fact, combined with the gradual decay of the catalytic current density over time during electrolysis (Figure S9, S13a and S13b), points toward a deactivation of the catalysts in operating conditions. In the case of complexes **1** and **2**, we observed a gradual deepening of the color of the electrolytic solution upon electrolysis. On the other hand, no precipitate and no particle formation could be observed during electrolysis, and a rinse test (see Figure S14 and ESI for details) proved negative. In addition, high resolution SEM images and EDX analysis of the electrode surface confirmed the absence of deposit at the electrode after electrolysis (Figure S15-S16). Monitoring complex **1** in CO_2 electrocatalytic conditions with in-situ IR-SEC revealed the gradual appearance of a new ν_{CO} stretch at 1893 cm^{-1} (Figure

S18). This points to the formation of a Co(I) carbonyl complex during catalytic turnover,[29] accumulating in electrocatalytic conditions and leading to deactivation. Such a catalyst deactivation by formation of a stable carbonyl complex has been previously reported for several molecular CO_2 reduction electrocatalysts.[29-30]

To further test that hypothesis, we attempted to regenerate the active catalyst by re-oxidation promoting the CO release. A 30 min controlled potential electrolysis at − 0.23 V was carried out immediately after 2 h CPE of complex **1** at -1.83 V under a CO_2 atmosphere in optimized catalytic conditions (0.11 M TFE). The decay of current in this re-oxidation step occurred concomitantly with a release of a substantial amount of CO in the headspace. Considering this amount and the charge stored under the form of the Co(I)-CO complex allows assigning over 95% of the passed current during electrolysis and a substantial increase of the total FY of 16% (Table S5). Regeneration of the active catalyst was confirmed by the CV of complex **1** after this re-oxidation step that is indistinguishable from that obtained from freshly prepared solutions (Figure S19).

Similar inhibition behavior was observed for complex **2**, also resulting in FYs close to unity (Figure S20; Table S5). Complex **2** however presented a faster decrease of current over CPE, suggesting that the CO inhibition was much faster than for complex **1** (Figure S20 and Figure S9). Despite that faster catalyst inhibition, we could also demonstrate the integrity of catalyst **2** after the oxidation step: initial catalytic activity could be essentially restored for a second CPE at -1.98 V carried out after the oxidation step (Figure S20 and table S6; see ESI for details).

The same procedures were applied for complex **3**. Contrary to what observed with complexes **1** and **2**, only trace amounts of CO were released (<1 % of FY) for **3** upon re-oxidation after 2 h CPE and catalytic activity could not be restored.

These data indicate that the deactivation is of different origin for complexes **1-2** and **3**: the former two are inhibited by the reversible binding of CO on the reduced catalyst, while the latter undergoes irreversible degradation. This can be explained by the electronic properties of the ligands. In the case of complex **3**, the strong electron density provided by the three thiolate ligands likely destabilizes the Co(I) state, as highlighted by the irreversibility of the Co$^{II/I}$ process in the CV. This results in a fast degradation of the catalyst, in agreement with the fast drop of current during electrolysis and low TONs. This deactivation was further confirmed by high-resolution SEM images and EDX analysis of the electrode surface after electrolysis, showing the deposition of nanoparticles containing Co and S (Figure S17). The decomposition of complex **3** to such a cobalt-sulfide material necessitates at least 3 electrons per complex decomposed, potentially explaining the lower FYs observed. In contrast, the presence of neutral bipyridine ligands in complexes **1** and **2** allows lowering the overall charge of the metal center and increased stabilization of the Co(I) species, which gets inhibited via the formation of a CO adduct. The faster inhibition reaction observed with complex **2** can be rationalized by the electron-donating -OMe substituents on the bipyridine ligand, which induce an increased electron density on the Co center and strengthen the metal to CO π−backdonation.

Reaction mechanism: In all cases HCOOH was the main product of the reduction, together with small amounts of CO and H_2. Our discussion will here mainly concern complex **1**, which is showing the best catalytic performances.

Two possible reaction pathways can lead to formate, via (i) the coordination of CO_2 to the Co(I) center affording a Co(III)-CO_2^{2-} intermediate followed by the reaction with weak Brønsted acids leading to formate after reorganization[1, 26, 31] or (ii) via the direct reaction of the Co(I) center with H^+ forming a Co(III)-H species, which can react with CO_2 to generate formate. To identify which reaction path is operational here, we investigated the kinetic parameters of this reaction in the case of complex **1**. The catalytic current correlates linearly with proton and catalyst concentration (Figure S6-S7 and S21), in agreement with a second-order dependency of the rate with proton concentration and a first-order dependency with catalyst concentration (see ESI for details). Furthermore, a first-order dependency of the rate with CO_2 concentration was observed (Figure S12). A primary kinetic isotope effect (KIE) of 8.2 was determined using water as a proton source, indicating that the rate-determining step (RDS) involves a proton transfer (Figure S23). This fairly large primary KIE suggests that the reaction takes place via the formation of Co-H species,[8c] in further agreement with the observation of H_2 as the second main product of the reaction. In that case, the employed proton source plays a key role in the competitive protonation of the M-H species affording H_2.[1, 31]

Yang and Kubiak have recently established a thermodynamic framework using the hydricity of the metal complex and the pK_a of the proton source as descriptors to rationalize the reactivity of metal hydrides with CO_2 and H^+ and the associated selectivity of the catalyst.[27, 32] We determined a hydricity (ΔG_{H^-}) value of 38 kcal mol^{-1} for the Co(III)-H species generated from **1** using the empirical equation developed by Kubiak *et. al*.[32] and standard reduction potential ($E_{1/2}^{I/I}$) (see ESI for details). This ΔG_{H^-} value is lower than that for formate in acetonitrile (44 kcal mol^{-1}), showing that the hydride transfer to CO_2 leading to formate is exergonic. The pK_a of TFE in CO_2-saturated acetonitrile of 25.1 exactly matches the pK_a defining the initial pH point from which selective CO_2 reduction can be achieved.[27] According to the thermodynamic product diagram illustrating metal hydride reactivity with protons and CO_2 in acetonitrile,[27] complex **1** operates in a zone where a competitive H_2 evolution occurs concomitantly to formate production. This also explains the larger amount of H_2 production for complex **1** in the presence of more acidic PhOH or water (i.e. carbonic acid in the presence of CO_2). Nevertheless, the proximity to the selective CO_2 reduction to formate area of the diagram ensures formate being the main product of the reaction. In the case of complexes **2** and **3** the hydricity of the corresponding Co(III)-H species (ΔG_{H^-} = 33 and 26 kcal mol^{-1}, respectively) is increased by the more electron-donating nature of the ligands and the selectivity for formate is thus increased, but at the expense of a higher thermodynamic cost.

The observation of CO as a minor product suggests that the catalyst can follow another reaction pathway involving the initial binding of CO_2 to reduced Co(I) center followed by a C-O bond cleavage mediated by protonation.[2b, 33]

These experimental findings along with DFT computations on complex **1**, allowed us to propose the overall reaction mechanism of CO_2 reduction to HCOOH, H_2 and CO as shown in Scheme 3.

The anodic potential shift in the CV in the presence of a proton source (Figure 2a and table 1) shows that the generation of the main active species involves a proton transfer. Our calculations indicate that the most favorable protonation site of both singly- (**1$_{red1}$**) and doubly- (**1$_{red2}$**) reduced complexes is the nitrogen atom of the pyridine-thiolate ligand (N_{PyS}). This is in full agreement with the reduced Co center favoring the thione form of the pyridine-thiolate ligand, confirmed by the shortening of the C-S bond of the ligand upon protonation by *ca.* 0.5 Å. The resulting species are **1$_{red1}$–NH** in a quartet state and **1$_{red2}$–NH** in a triplet state (the corresponding low-spin structure is 15.4 kcal mol^{-1} higher in energy, see Table S7). Intramolecular proton transfer from N_{PyS} to the Co center has a computed transition state (TS) barrier of 34.8 kcal mol^{-1}, indicating that the formation of Co(III)-H hydride species cannot occur *via* this pathway, in line with the stabilization of the pyridine-thiolate ligand in the thione form upon protonation mentioned above. Instead, direct protonation of the Co^I site by TFE is more favorable to occur with a TS barrier of 20.1 kcal mol^{-1}, affording the Co(III)–H hydride species **1-CoH** (MOs shown in Figure S24). The high activation energy is in agreement with the hydride formation being the RDS step. The transition state structure for this second proton transfer highlights the stabilization of the incoming TFE by hydrogen bonding with the protonated pyridine (Figure S25). The Co^{III}–H can promote a hydride transfer to CO_2 to generate the Co-HCO_2 complex **1-HCO$_2$**, with a transition state barrier of 14.5 kcal mol^{-1} (**TS$_1$** structure in Figure S23a), which upon CO_2 insertion converts to intermediate **1-OCHO** (ΔG = -3.2 kcal mol^{-1}). Further protonation leads to the release of HCOOH and the recovery of catalyst **1**.

The competitive formation of hydrogen is proposed to occur via the direct protonation of the Co(III)–H bond by a TFE molecule, leading to an H–H bond in a CoH_2 adduct. The computed transition state barrier is 20.2 kcal mol^{-1}, in agreement with the findings of formate being the major product. The TFE interacts via hydrogen-bonding with the protonated N_{PyS}, facilitating the proton transfer to the Co–H unit (**TS$_2$** structure in Figure S26b). Our calculations could not locate a transition state involving the Co–H and N–H units and implying an intramolecular pathway for the H_2 formation.

Last, CO_2 binding on complex **1$_{red2}$-NH** in a η_1-CO_2(C) fashion is endergonic by 11 kcal mol^{-1}, affording the species **1$_{red2}$-CO$_2$**. Binding in a η_2-CO_2(C,O) or η_1-OCO manner is 10.4 and 17.2 kcal mol^{-1} energetically less favored. Intramolecular proton transfer from the protonated N_{PyS} ligand yields a carboxylate intermediate **1-COOH** with a TS barrier of only 2.5 kcal mol^{-1}. The easy intramolecular proton transfer observed here is consistent with the destabilization of the thione form of the ligands upon oxidation of the Co center to Co(III). This further highlights the adaptability of the pyridine-thiolate ligand and its influence on the pyridine nitrogen protonation: low Co oxidation states favor the thione form and the protonation of the nitrogen while high oxidation states favor the thiolate form and deprotonated pyridine.

In the presence of TFE, **1-COOH** undergoes a heterolytic cleavage of the C–O bond ($\Delta G^{\ddagger}$ = 25.6 kcal mol^{-1}), to produce the CO-bound complex **1-CO** and water (MOs are shown in Figures S27-S28). **1-CO** can release CO and regenerate complex **1** or alternatively be further reduced by 2 electrons to afford the Co(I)-CO complex **1$_{red2}$-CO**. This species has a characteristic CO stretching at 1907 cm^{-1}, in close agreement with the deactivation species observed in IR-SEC experiments.
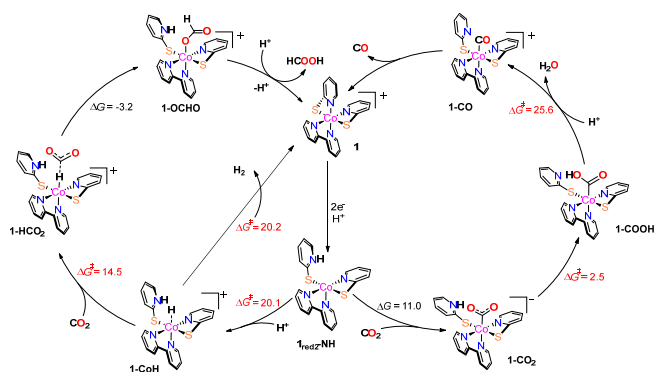
Scheme 3: Proposed reaction mechanism for the generation of HCOOH, H_2 and CO. The relative Gibbs free energies (ΔG, kcal mol^{-1}) and transition state barriers ($\Delta G^{\ddagger}$, kcal mol^{-1}) are given relative to the preceding intermediate

Conclusion

This work allowed isolating a series of highly active Co-based CO_2 electroreduction catalysts. We achieved the conversion of CO_2 to HCOOH as the major product with very low overpotential by tuning the electronic properties of the metal centers using pyridine-thiolate ligands. Benchmarking of these complexes allowed identifying complex **1** as one of the best catalysts amongst all CO_2 to HCOOH molecular electrocatalysts to date. We identified here that the formation of a stable carbonyl complex was at the origin of the catalyst deactivation. We demonstrated the possibility to regenerate the active catalyst by re-oxidation of such carbonyl resting states, promoting the CO ligand release. The electronic and mechanistic understanding provided by this study highlights the interest of using thiolate-based ligands in the context of CO_2 reduction.

Acknowledgements

References

[1]   R. Francke, B. Schille, M. Roemelt, *Chem. Rev.* **2018**, *118*, 4631-4701.

[2]   a) J. M. Smieja, M. D. Sampson, K. A. Grice, E. E. Benson, J. D. Froehlich, C. P. Kubiak, *Inorg. Chem.* **2013**, *52*, 2484-2491; b) J. Hawecker, J.-M. Lehn, R. Ziessel, *J. Chem. Soc., Chem. Commun.* **1984**, 328-330.

[3]   a) C. W. Machan, M. D. Sampson, C. P. Kubiak, *J. Am. Chem. Soc.* **2015**, *137*, 8564-8571; b) B. A. Johnson, S. Maji, H. Agarwala, T. A. White, E. Mijangos, S. Ott, *Angew. Chem. Int. Ed.* **2016**, *55*, 1825-1829.

[4]   P. Kang, C. Cheng, Z. Chen, C. K. Schauer, T. J. Meyer, M. Brookhart, *J. Am. Chem. Soc.* **2012**, *134*, 5500-5503.

[5]   a) C. Caix, S. Chardon-Noblat, A. Deronzier, *J. Electroanal. Chem.* **1997**, *434*, 163-170; b) T. K. Todorova, T. N. Huan, X. Wang, H. Agarwala, M. Fontecave, *Inorg. Chem.* **2019**, *58*, 6893-6903.

[6]   a) M. Bourrez, F. Molton, S. Chardon-Noblat, A. Deronzier, *Angew. Chem. Int. Ed.* **2011**, *50*, 9903-9906; b) M. D. Sampson, A. D. Nguyen, K. A. Grice, C. E. Moore, A. L. Rheingold, C. P. Kubiak, *J. Am. Chem. Soc.* **2014**, *136*, 5460-5471; c) B. Reuillard, K. H. Ly, T. E. Rosser, M. F. Kuehnel, I. Zebger, E. Reisner, *J. Am. Chem. Soc.* **2017**, *139*, 14425-14435.

[7]   a) C. Costentin, S. Drouet, M. Robert, J.-M. Savéant, *Science* **2012**, *338*, 90; b) M. Hammouche, D. Lexa, M. Momenteau, J. M. Saveant, *J. Am. Chem. Soc.* **1991**, *113*, 8455-8466; c) C. Costentin, M. Robert, J.-M. Savéant, *Acc. Chem. Res.* **2015**, *48*, 2996-3006; d) A. W. Nichols, S. Chatterjee, M. Sabat, C. W. Machan, *Inorg. Chem.* **2018**, *57*, 2111-2121.

[8]   a) D. C. Lacy, C. C. L. McCrory, J. C. Peters, *Inorg. Chem.* **2014**, *53*, 4980-4988; b) N. Elgrishi, M. B. Chambers, M. Fontecave, *Chem. Sci.* **2015**, *6*, 2522-2531; c) S. Roy, B. Sharma, J. Pécaut, P. Simon, M. Fontecave, P. D. Tran, E. Derat, V. Artero, *J. Am. Chem. Soc.* **2017**, *139*, 3685-3696.

[9]   a) M. F. Kuehnel, K. L. Orchard, K. E. Dalle, E. Reisner, *J. Am. Chem. Soc.* **2017**, *139*, 7217-7223; b) D. Hong, Y. Tsukakoshi, H. Kotani, T. Ishizuka, T. Kojima, *J. Am. Chem. Soc.* **2017**, *139*, 6538-6541.

[10]   H. Takeda, C. Cometto, O. Ishitani, M. Robert, *ACS Catal.* **2017**, *7*, 70-88.

[11]   a) M. Can, F. A. Armstrong, S. W. Ragsdale, *Chem. Rev.* **2014**, *114*, 4149-4174; b) R. Hille, J. Hall, P. Basu, *Chem. Rev.* **2014**, *114*, 3963-4038; c) J.-H. Jeoung, H. Dobbek, *Science* **2007**, *318*, 1461; d) H. Dobbek, L. Gremer, R. Kiefersauer, R. Huber, O. Meyer, *Proc. Nat. Acad. Sci.* **2002**, *99*, 15971; e) H. Dobbek, L. Gremer, O. Meyer, R. Huber, *Proc. Nat. Acad. Sci.* **1999**, *96*, 8884.

[12]   a) M. J. Romão, *Dalton Trans.* **2009**, 4053-4068; b) L. B. Maia, J. J. G. Moura, I. Moura, *J. Biol. Inorg. Chem.* **2015**, *20*, 287-309.

[13]   a) T. Fogeron, T. K. Todorova, J.-P. Porcher, M. Gomez-Mingot, L.-M. Chamoreau, C. Mellot-Draznieks, Y. Li, M. Fontecave, *ACS Catal.* **2018**, *8*, 2030-2038; b) T. Fogeron, P. Retailleau, M. Gomez-Mingot, Y. Li, M. Fontecave, *Organometallics* **2019**, *38*, 1344-1350; c) S. Dey, M. E. Ahmed, A. Dey, *Inorg. Chem.* **2018**, *57*, 5939-5947; d) M. E. Ahmed, A. Rana, R. Saha, S. Dey, A. Dey, *Inorg. Chem.* **2020**, *59*, 5292-5302.

[14]   Z. Han, L. Shen, W. W. Brennessel, P. L. Holland, R. Eisenberg, *J. Am. Chem. Soc.* **2013**, *135*, 14659-14669.

[15]   M. Kita, K. Yamanari, Y. Shimura, *Bull. Chem. Soc. Jpn.* **1989**, *62*, 3081-3088.

[16]   K. J. Franz, L. H. Doerrer, B. Spingler, S. J. Lippard, *Inorg. Chem.* **2001**, *40*, 3774-3780.

[17]   a) A. Chapovetsky, T. H. Do, R. Haiges, M. K. Takase, S. C. Marinescu, *J. Am. Chem. Soc.* **2016**, *138*, 5765-5768; b) S. Fukuzumi, S. Mandal, K. Mase, K. Ohkubo, H. Park, J. Benet-Buchholz, W. Nam, A. Llobet, *J. Am. Chem. Soc.* **2012**, *134*, 9906-9909.

[18]   S. G. Rosenfield, P. K. Mascharak, S. K. Arora, *Inorg. Chim. Acta* **1987**, *129*, 39-46.

[19]   S. G. Rosenfield, H. P. Berends, L. Gelmini, D. W. Stephan, P. K. Mascharak, *Inorg. Chem.* **1987**, *26*, 2792-2797.

[20]   M. Gennari, D. Brazzolotto, S. Yu, J. Pécaut, C. Philouze, M. Rouzières, R. Clérac, M. Orio, C. Duboc, *Chem. Eur. J.* **2015**, *21*, 18770-18778.

[21]   M. Okuno, M. Kita, K. Kashiwabara, J. Fujita, *Chem. Lett.* **1989**, *18*, 1643-1646.

[22]   a) D. Brazzolotto, M. Gennari, N. Queyriaux, T. R. Simmons, J. Pécaut, S. Demeshko, F. Meyer, M. Orio, V. Artero, C. Duboc, *Nat. Chem.* **2016**, *8*, 1054; b) S. Roy, T. L. Groy, A. K. Jones, *Dalton Trans.* **2013**, *42*, 3843-3853.

[23]   K. T. Ngo, M. McKinnon, B. Mahanti, R. Narayanan, D. C. Grills, M. Z. Ertem, J. Rochford, *J. Am. Chem. Soc.* **2017**, *139*, 2604-2618.

[24]   a) C. Costentin, S. Drouet, M. Robert, J.-M. Savéant, *J. Am. Chem. Soc.* **2012**, *134*, 11235-11242; b) C. Costentin, M. Robert, J.-M. Savéant, *Chem. Soc. Rev.* **2013**, *42*, 2423-2436.

[25]   A. Taheri, E. J. Thompson, J. C. Fettinger, L. A. Berben, *ACS Catal.* **2015**, *5*, 7140-7151.

[26] L. Chen, Z. Guo, X.-G. Wei, C. Gallenkamp, J. Bonin, E. Anxolabéhère-Mallart, K.-C. Lau, T.-C. Lau, M. Robert, *J. Am. Chem. Soc.* **2015**, *137*, 10918-10921.

[27] B. M. Ceballos, J. Y. Yang, *Proc. Nat. Acad. Sci.* **2018**, *115*, 12686.

[28] F.-W. Liu, J. Bi, Y. Sun, S. Luo, P. Kang, *ChemSusChem* **2018**, *11*, 1656-1663.

[29] S. Fernández, F. Franco, C. Casadevall, V. Martin-Diaconescu, J. M. Luis, J. Lloret-Fillol, *J. Am. Chem. Soc.* **2020**, *142*, 120-133.

[30] a) J. Schneider, H. Jia, J. T. Muckerman, E. Fujita, *Chem. Soc. Rev.* **2012**, *41*, 2036-2051; b) E. Fujita, C. Creutz, N. Sutin, D. J. Szalda, *J. Am. Chem. Soc.* **1991**, *113*, 343-353; c) J. D. Froehlich, C. P. Kubiak, *J. Am. Chem. Soc.* **2015**, *137*, 3565-3573.

[31] B. Mondal, A. Rana, P. Sen, A. Dey, *J. Am. Chem. Soc.* **2015**, *137*, 11214-11217.

[32] K. M. Waldie, A. L. Ostericher, M. H. Reineke, A. F. Sasayama, C. P. Kubiak, *ACS Catal.* **2018**, *8*, 1313-1324.

[33] M. L. Clark, P. L. Cheung, M. Lessio, E. A. Carter, C. P. Kubiak, *ACS Catal.* **2018**, *8*, 2021-2029.